Heterocyclic Systems Containing Tin(IV). 11.[1] Stannocanes Cl/Br/I/Me–(Me)Sn(SCH_2CH_2)$_2$X (X = O, S, NMe): Synthesis and Structural and Vibrational Data. A Semiquantitative Investigation of the Energy Gain of Pentacoordinate Tin in Terms of Frontier Orbitals†

Ute Kolb, Mike Beuter, Matthias Gerner, and Martin Dräger*

Institute für Anorganische Chemie und Analytische Chemie der Johannes Gutenberg-Universität, D-55099 Mainz, Germany

Received May 26, 1994®

The stannocanes mentioned in the title have been synthesized from $MeSnHal_3$ and ($HSCH_2CH_2$)$_2$X. Crystal structure determinations and vibrational transitions of the coordination polyhedra around tin are given. The 12 compounds are compared with the 9 compounds $Cl_2/Br_2/I_2$–Sn(SCH_2CH_2)$_2$X (X = NMe, O, S) investigated in a previous study. Apart from one molecule with heptacoordinated tin, the other compounds comprise pentacoordinated tin on a "path" from a tetrahedron to a trigonal bipyramid. The path is discussed in terms of the molecular orbitals of the three-center, four-electron interaction X···Sn–Cl/Br/I/Me. By the use of standard single-bond distances, vibrations, and bond energies, and with the help of Morse potentials, the structural and vibrational data are transformed into semiquantitative energy diagrams of the occupied equatorial and axial orbitals. The energy differences between these orbitals and those of a tetrahedral configuration are added up to give the total energy gain of each compound (energy coordinate) and are plotted versus an angle sum of the respective trigonal bipyramid (configurational coordinate). The total energy gain from the structural and vibrational data includes an energy contribution from the LUMO of the three-center interaction. A model is presented in which an enhanced electronegativity of the equatorial and axial ligands inhibits the formation of a pentacoordinate structure. The drive for pentacoordination (σ-Lewis acidity) results from a movable charge which populates the LUMO (π-Lewis acidity). The movable charge originates from the lone pairs of the halides and chalcogenides, from the π-electrons of aromatic rings, or from the hyperconjugation in the case of the methyl group. This model contradicts the generally accepted opinion that electronegativity promotes pentacoordination. With regard to the presented model, a short discussion of hypervalency for the other group 14 elements and a mention of the broad subject of bimolecular nucleophilic attack are given.

Introduction

Compelled by the longstanding problem of hypervalency of group 14 and group 15 elements,[2] especially of tin(IV),[3] we discussed in a previous paper[1] some structural and spectroscopic features of the three-compound series $Cl_2/Br_2/I_2$–Sn(SCH_2CH_2)$_2$X with X = NMe (**1**), O (**2**), and S (**3**) (Chart 1). The nine compounds comprise molecules in which the tin atom approaches trigonal-bipyramidal pentacoordination with two sulfurs and Hal(eq) as equatorial ligands and with X and Hal(ax) as axial ligands. The last two bonds were described by means of the three-center, four-electron interaction X···Sn–Hal, for which a qualitative MO description in terms of frontier orbitals was given.[4] The path from a tetrahedron to a trigonal bipyramid is controlled by four electronic factors. Three of these factors—the donor strength of X, the electronegativity of Hal(ax), and the lone pair interaction of Hal(ax)—were discussed in detail.[1] In this study, the influence of the fourth

Chart 1

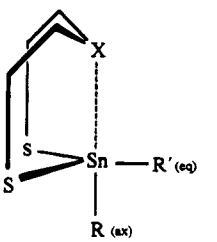

X	R(ax)R′(eq)
NMe	Cl_2 (**1a**), Br_2 (**1b**), I_2 (**1c**)
O	Cl_2 (**2a**), Br_2 (**2b**), I_2 (**2c**)
S	Cl_2 (**3a**), Br_2 (**3b**), I_2 (**3c**)
O	ClMe (**4a**), BrMe (**4b**), IMe (**4c**)
S	ClMe (**5a**), BrMe (**5b**), IMe (**5c**)
NMe	ClMe (**6a**), BrMe (**6b**), IMe (**6c**)
O	Me_2 (**7a**)
S	Me_2 (**8a**)
NMe	Me_2 (**9a**)

† This paper includes parts of the intended Ph.D. theses of U. Kolb and M. Beuter.

® Abstract published in *Advance ACS Abstracts,* October 1, 1994.

(1) Part 10: Kolb, U.; Beuter, M.; Dräger, M. *Inorg. Chem.* **1994,** *33,* 4522.

(2) Holmes, R. R. *Prog. Inorg. Chem.* **1984,** *32,* 119.

(3) Cf. the references cited in recent articles: (a) Jastrzebski, J. T. B. H.; van der Schaaf, P. A.; Boersma, J.; van Koten, G. *Organometallics* **1982,** *11,* 1521. (b) Dakternieks, D.; Zhu, H.; Masi, D.; Mealli, C. *Inorg. Chem.* **1992,** *31,* 3601. (c) Dostal, S.; Stoudt, S. J.; Fanwick, P.; Sereatan, W. F.; Kahr, B.; Jackson, J. E. *Organometallics* **1993,** *12,* 2284.

0276-7333/94/2313-4413$04.50/0

Table 1. Bond Lengths, Bond Angles, and Torsion Angles of the Coordination Polyhedra at the Central Tin Atom and for the Eight-Membered Rings in ClMeSn(SCH$_2$CH$_2$)$_2$O (4a), BrMeSn(SCH$_2$CH$_2$)$_2$O (4b), IMeSn(SCH$_2$CH$_2$)$_2$O (4c), and Me$_2$Sn(SCH$_2$CH$_2$)$_2$O (7a)

	4a (Hal = Cl)	4b (Hal = Br)	4c (Hal = I)	7a (Hal = Me)	
		(a) Coordination Polyhedra			
		Bond Lengths (Å)[a]			
Sn–Hal (ax)	2.413(1)	2.561(1)	2.762(1)	2.133(8)	
Sn–Me(eq)	2.17(4)	2.126(7)	2.143(6)	2.119(7)	
Sn···O	2.42(2)	2.440(4)	2.466(3)	2.774(5)	
Sn–S(1)	2.381(7)	2.393(2)	2.396(1)	2.405(1)	
Sn–S(2)	2.388(9)	2.393(2)	2.390(1)	2.405(1)	
		Bond Angles (deg)			
Hal(ax)–Sn···O	168.3(5)	166.5(1)	167.0(1)	163.6(3)	
Hal(ax)–Sn–Me(eq)	103(1)	104.6(2)	106.0(2)	114.4(3)	
Hal(ax)–Sn–S(1)	96.0(3)	95.8(1)	96.5(1)	94.4(3)/106.3(3)[c]	
Hal(ax)–Sn–S(2)	95.3(3)	96.3(1)	96.5(1)	106.3(3)/94.4(3)[c]	
O···Sn–Me(eq)	89(1)	88.9(2)	86.9(2)	80.3(2)	
O···Sn–S(1)	78.4(4)	77.9(1)	77.7(1)	72.5(1)	
O···Sn–S(2)	79.1(5)	77.3(1)	77.0(1)	72.5(1)	
Me(eq)–Sn–S(1)	115(1)	114.1(2)	114.1(2)	112.0(1)	
Me(eq)–Sn–S(2)	118(1)	118.0(2)	116.8(2)	112.0(1)	
S(1)–Sn–S(2)	121.1(3)	121.0(1)	120.9(1)	116.6(1)	
		(b) Eight-Membered Rings			
		Bond Lengths (Å)			
S(1)–C(1)	1.82(5)/1.82(5)[b]	1.82(1)	1.85(1)	1.82(1)	
C(1)–C(2)	1.49(7)/1.49(7)[b]	1.51(1)	1.44(1)	1.55(1)	
C(2)–O	1.45(4)/1.45(5)[b]	1.43(1)	1.43(1)	1.41(1)	
O–C(3)	1.44(4)	1.43(1)	1.45(1)	1.41(1)	
C(3)–C(4)	1.49(4)	1.49(1)	1.47(1)	1.55(1)	
C(4)–S(2)	1.82(3)	1.84(1)	1.83(1)	1.82(1)	
		Bond Angles (deg)			
Sn–S(1)–C(1)	96(2)/102(2)[b]	98.0(3)	97.4(2)	102.2(2)	
S(1)–C(1)–C(2)	109(3)/118(3)[b]	112.2(5)	113.2(4)	111.7(3)	
C(1)–C(2)–O	106(3)/105(3)[b]	109.2(5)	109.7(5)	106.9(5)	
C(2)–O–C(3)	102(2)/123(2)[b]	113.4(5)	114.0(4)	111.9(4)	
O–C(3)–C(4)	107(2)	108.8(5)	109.7(4)	106.9(4)	
C(3)–C(4)–S(2)	112(3)	110.7(4)	111.2(3)	111.7(3)	
C(4)–S(2)–Sn	98(1)	95.8(2)	96.6(2)	102.2(2)	
		Torsion Angles (deg)			
S(2)–Sn–S(1)–C(1)	96(2)/70(2)[b]	−92.1(3)	−89.4(2)	−81.7(2)	
Sn–S(1)–C(1)–C(2)	−59(3)/29(4)[b]	53.2(5)	53.0(5)	61.1(4)	chair
S(1)–C(1)–C(2)–O	66(4)/−54(4)[b]	−56.8(6)	−58.8(6)	−62.2(5)	
C(1)–C(2)–O–C(3)	−159(3)/−91.4(4)[b]	165.5(6)	166.1(6)	153.7(7)	
C(2)–O–C(3)–C(4)	162(3)/−178(3)[b]	−162.3(6)	−159.1(5)	−161.0(5)	
O–C(3)–C(4)–S(2)	−63(8)	58.6(6)	57.8(5)	62.2(5)	chair
C(3)–C(4)–S(2)–Sn	51(2)	−59.2(4)	−58.8(5)	−61.1(4)	
C(4)–S(2)–Sn–S(1)	−89(1)	97.2(3)	96.6(2)	86.8(2)	

[a] Shortest intermolecular distances: **4a**, d(Sn···O) = 4.545 Å; **4b**, d(Sn···S) = 4.507 Å; **4c**, d(Sn···S) = 4.538 Å; **7a**, d(Sn···S) = 4.839 Å. [b] Splitting of C(1) and C(2), respectively, in **4a**. [c] Disorder of Me(ax) in **7a**.

electronic factor, the type of equatorial ligand, shall be considered in a semiquantitative manner. For the purpose of this discussion, we synthesized the methyl compounds Cl/Br/I/Me–(Me)Sn(SCH$_2$CH$_2$)$_2$X with X = O (**4** and **7a**), with X = S (**5** and **8a**), and with X = NMe (**6** and **9a**[5]) (Chart 1) and compare their crystal structures (all compounds except **5c** and **6**) and vibrational data with those of the series **1**–**3**.

In fact, on the basis of the study carried out in ref 1, this paper shall present a new concept on hypervalency and possibly also on the whole subject of bimolecular nucleophilic attack: three-center interactions controlled by π-Lewis acidity.

(4) For an analogous qualitative description of stannate anions see: Suzuki, M.; Son, I.-H.; Noyori, R.; Masuda, H. *Organometallics* **1990**, *9*, 3043.

(5) (a) Synthesis: Mügge, C.; Jurkschat, K.; Tzschach, A.; Zschunke, A. *J. Organomet. Chem.* **1979**, *164*, 135. (b) Crystal structure determination: Dräger, M. *J. Organomet. Chem.* **1983**, *251*, 209. Swisher, R. G.; Holmes, R. R. *Organometallics* **1984**, *3*, 365.

Results

Molecular Structures. The structure determinations of the six compounds **4a**–**c**, **7a**, and **5a**,**b** reveal pentacoordinate tin due to a transannular coordination by the donor atom O or S. In addition to this *intra*molecular coordination site, the compound Me$_2$Sn(SCH$_2$CH$_2$)$_2$S (**8a**) has two *inter*molecular coordination sites and exhibits heptacoordination for tin. The geometrical properties of these seven compounds and, for comparison, of Me$_2$Sn(SCH$_2$CH$_2$)$_2$NMe (**9a**)[5b] are given in Tables 1 and 2. For the compound I–(Me)Sn(SCH$_2$CH$_2$)$_2$S (**5c**) and for the compounds **6**, a structure determination was not possible due to the lack of single crystals.

Pentacoordination and Ring Conformation. In the compound series **4a**–**c**, **7a** and **5a**,**b** the individual members differ only slightly. Figure 1 gives exemplary plots of the two bromine-substituted cases. All compounds containing a coordinating oxygen atom exhibit a chair–chair conformation of the eight-membered ring (Figure 1, top), while for the compounds with a sulfur

Table 2. Bond Lengths, Bond Angles, and Torsion Angles of the Coordination Polyhedra at the Central Tin Atom and for the Eight-Membered Rings in ClMeSn(SCH_2CH_2)$_2$S (5a), BrMeSn(SCH_2CH_2)$_2$S (5b), $Me_2Sn(SCH_2CH_2)_2S$ (8a), and, for Comparison, $Me_2Sn(SCH_2CH_2)NMe$ (9a)[a]

	5a (Hal = Cl)	5b (Hal = Br)	8a (Hal = Me)	9a (Hal = Me)	
		(a) Coordination Polyhedra			
		Bond Lengths (Å)[b]			
Sn–Hal(ax)	2.444(1)	2.582(1)	2.147(3)	2.16(1)	
Sn–Me(eq)	2.122(3)	2.138(6)	2.134(3)	2.14(1)	
Sn···S(2)	2.863(1)	2.835(2)	3.514(1)	2.566(6)	
Sn–S(1)	2.401(1)	2.404(2)	2.435(1)	2.428(2)	
Sn–S(3)	2.410(1)	2.413(2)	2.435(1)	2.428(2)	
		Bond Angles (deg)			
Hal(ax)–Sn···S(2)	168.64(3)	168.52(4)	169.3(1)	165.8(3)	
Hal(ax)–Sn–Me(eq)	99.0(1)	98.7(2)	115.6(1)	107.2(4)	
Hal(ax)–Sn–S(1)	88.96(3)	88.50(5)	103.6(1)	93.0(3)	
Hal(ax)–Sn–S(3)	97.67(3)	97.44(4)	104.2(1)	97.1(3)	
S(2)···Sn–Me(eq)	91.5(1)	91.9(2)	75.1(1)	86.9(3)	
S(2)···Sn–S(1)	81.99(3)	82.18(6)	71.87(2)	77.9(2)	
S(2)···Sn–S(3)	81.04(2)	81.59(5)	68.81(2)	78.2(2)	
Me(eq)–Sn–S(1)	120.6(1)	121.4(2)	107.4(1)	120.2(3)	
Me(eq)–Sn–S(3)	117.4(1)	116.6(2)	118.2(1)	114.2(3)	
S(1)–Sn–S(3)	119.63(3)	119.98(5)	106.57(3)	118.3(1)	
		(b) Eight-Membered Rings			
		Bond Lengths (Å)			
S(1)–C(1)	1.813(3)	1.823(7)	1.826(3)	1.78(1)	
C(1)–C(2)	1.519(5)	1.51(1)	1.515(4)	1.56(2)	
C(2)–S(2)	1.807(3)	1.801(7)	1.821(3)	1.49(1)	
S(2)–C(3)	1.809(3)	1.806(7)	1.805(3)	1.46(1)	
C(3)–C(4)	1.522(5)	1.534(9)	1.520(4)	1.55(1)	
C(4)–S(3)	1.825(3)	1.831(7)	1.815(3)	1.82(1)	
		Bond Angles (deg)			
Sn–S(1)–C(1)	103.7(1)	104.1(2)	104.9(1)	105.7(4)	
S(1)–C(1)–C(2)	114.4(2)	112.9(4)	114.7(2)	111.8(7)	
C(1)–C(2)–S(2)	109.5(2)	110.7(4)	112.4(2)	110.3(8)	
C(2)–S(2)–C(3)	102.7(2)	103.0(3)	102.3(2)	110.9(7)	
S(2)–C(3)–C(4)	113.6(2)	113.1(4)	114.9(2)	111.2(6)	
C(3)–C(4)–S(3)	113.8(2)	113.9(4)	114.5(2)	114.8(6)	
C(4)–S(3)–Sn	101.5(1)	101.2(2)	102.7(1)	104.6(3)	
		Torsion Angles (deg)			
S(3)–Sn–S(1)–C(1)	89.9(1)	89.9(2)	−93.8(1)	69.7(4)	chair
Sn–S(1)–C(1)–C(2)	−52.4(2)	−50.7(4)	78.9(2)	−29.2(8)	chair
S(1)–C(1)–C(2)–S(2)	70.9(3)	70.8(5)	−74.8(2)	60.1(8)	chair
C(1)–C(2)–S(2)–C(3)	−144.2(2)	−146.6(5)	120.6(2)	−172.7(9)	chair
C(2)–S(2)–C(3)–C(4)	70.6(2)	69.9(5)	−76.1(2)	66.2(8)	boat
S(2)–C(3)–C(4)–S(3)	62.1(3)	62.0(5)	−62.3(2)	53.5(8)	boat
C(3)–C(4)–S(3)–Sn	−61.6(2)	−60.6(4)	84.9(2)	−27.8(7)	boat
C(4)–S(3)–Sn–S(1)	−46.0(1)	−47.3(2)	19.0(1)	−67.6(4)	boat

[a] See ref 5b. [b] Shortest intermolecular distances: **5a**, d(Sn···Cl) = 4.131 Å; **5b**, d(Sn···Br) = 4.253 Å; **8a**, d(Sn···S) = 3.678 Å.

donor boat–chair conformations are found (Figure 1, bottom). The compound **7a** has a perfect mirror plane due to its space group, on which plane Me(eq), Sn, and O are located. The axial methyl group is slightly disordered perpendicular to this plane. The other three compounds of the series **4** contain a mirror plane with minor deviations. In the compound Cl–(Me)Sn(SCH_2-$CH_2)_2$O (**4a**) a splitting of both atoms C(1) and C(2) is observed. The analysis of the sites of the disordered atoms shows that in the same crystal, in addition to the chair–chair ring, a ring with a boat–chair conformation exists (Table 1).

In the compounds with a chair–chair ring, the endocyclic angle is the greatest of the equatorial angles at tin. In the compounds with a boat–chair ring, one of the endo–exo equatorial angles is the greatest of the angles at tin. This demonstrates that in addition to the four electronic factors mentioned in the Introduction, a steric factor should be considered in controlling the path.[1]

Heptacoordination. As mentioned above, the compound $Me_2Sn(SCH_2CH_2)_2S$ (**8a**) exhibits heptacoordinate tin due to one intramolecular coordination (S(2)···Sn = 3.514(1) Å, Pauling-type bond order (BO) 0.03) and two intermolecular coordinations (S(1)′···Sn = 3.678(2) Å, BO = 0.07; S(3)″···Sn = 4.097(2) Å, BO = 0.03). The resulting network is shown in Figure 2. The Pauling-type bond order BO is calculated from the difference Δd between the distance d and a single-bond distance standard d(std)[7] by means of eq 1. The term s is

$$\mathrm{BO} = 10^{-(1.41(\Delta d)/s)} \quad (1)$$

different for intramolecular bonds (s = 1.0) and for intermolecular bonds (s = 1.6). For details, see refs 1 and 6.

The three additional coordination sites unfold the former tetrahedron into a tricapped tetrahedron. The

(6) Pauling, L. *The Nature of the Chemical Bond*, 3rd ed.; Cornell University Press: Ithaca, NY, 1960; Chapter 7. Dunitz, J. D. *X-Ray Analysis and the Structure of Organic Molecules*; Cornell University Press: Ithaca, NY, 1979; Chapter 7.

(7) Sum of radii without correction for electronegativity: O'Keeffe, M.; Brese, N. E. *J. Am. Chem. Soc.* **1991**, *113*, 3226. The distance d(Sn–I) was taken from a crystal structure determination of Mes_3-SnI: Schneider-Koglin, C.; Dräger, M. Unpublished data.

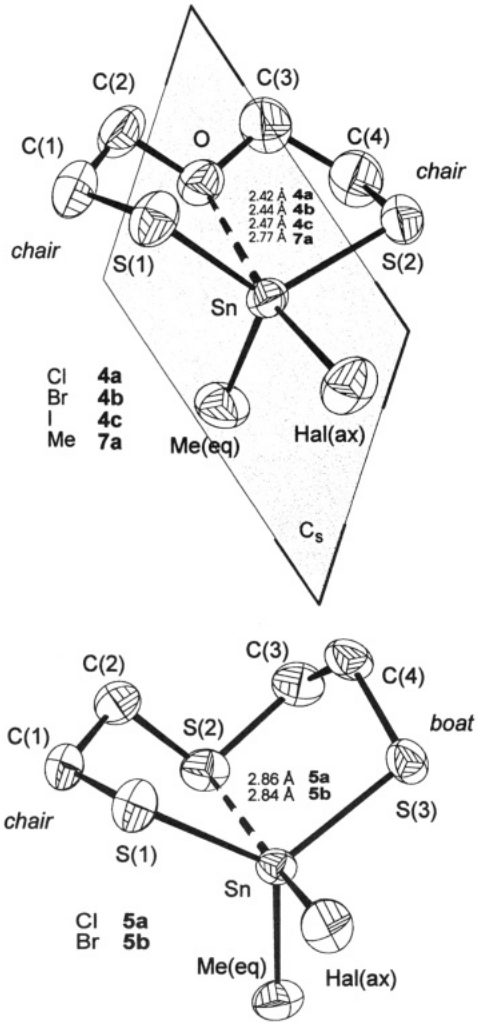

Figure 1. Intramolecular coordination in the compounds Hal(Me)Sn(SCH_2CH_2)$_2$X (Hal = Cl (**4a**, **5a**), Br (**4b**, **5b**), I (**4c**), Me (**7a**)). Labels of atoms are as given in Tables 1 and 2. ORTEP drawings are given of **4b** (top) and **5b** (bottom). The thermal ellipsoids are shown at the 50% probability level. Hydrogen atoms are omitted for better clarity. The mirror plane C_s in **4b** is outlined.

resulting polyhedron can also be described as the trigonal antiprism S(1)S(3)Me(ax)−Sn−S(2)S(1)′S(3)″ which is monocapped by Me(eq) above the triangulated face S(2)S(1)′S(3)″. This description is equivalent to the configuration of the heptacoordinate compounds **10**[3c] (Chart 2). The compounds **8a** and **10** are on a path from

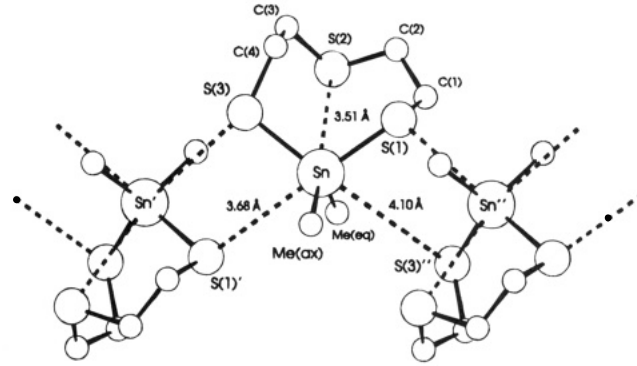

Figure 2. *Intra-* and *Inter*molecular coordination in the compound $Me_2Sn(SCH_2CH_2)_2S$ (**8a**). Labels of atoms are as given in Table 2. The respective symmetry operators are x, y, z for the center molecule, $0.5 - x, -0.5 + y, 0.5 - z$ for the molecule Sn′ on the left, and $0.5 - x, 0.5 + y, 0.5 - z$ for the molecule Sn″ on the right. A PLUTO drawing without hydrogen atoms has been chosen for better clarity.

Chart 2[a]

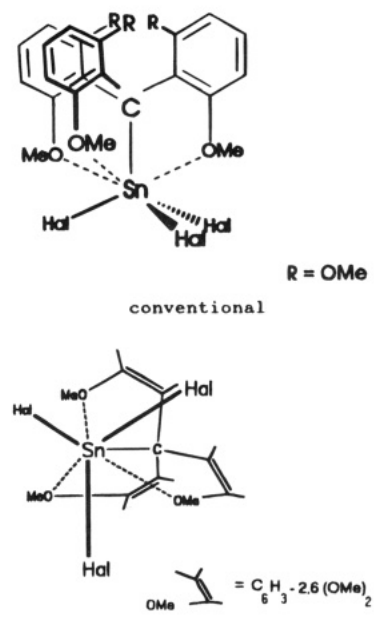

[a] Legend: Hal = Cl (**10a**), Br (**10b**), I (**10c**), F (**10d**).

a tetrahedron to a monocapped octahedron. The three axial bonds Sn−S(1)/S(3)/Me(ax) become the three 4-fold axes of the octahedron (angles between them 3 × 90°). The equatorial bond Sn−Me(eq) becomes one of the four 3-fold axes of the octahedron (angles to the 4-fold axes 3 × 125.27°).

Vibrational Data. A full set of assigned IR and Raman transitions <600 cm^{-1} for the compound series **4**−**6** and for **7a**, **8a**, and **9a** has been determined. Table 3 gives the five stretching vibrations of the coordination polyhedra for tin. For other data, see the supplementary material.

Discussion

Three-Center Interaction. In ref 1 the path from a tetrahedron to a trigonal bipyramid was investigated by means of the distances d and the stretching vibrations ν of the axial three-center interactions X···Sn−R(ax). These data were referenced to standard single-bond distances and vibrations. The deviations Δd and

(8) Me_3SnF, gas phase: Licht, K.; Geissler, H.; Koehler, P.; Hottmann, K.; Schnorr, H.; Kriegsmann, H. *Z. Anorg. Allg. Chem.* **1971**, *385*, 271. Me_3Sn−Cl/Br/I, cyclohexane solution: Clark, R. J. H.; Davies, A. G.; Puddephatt, R. J. *J. Chem. Soc. A* **1968**, 1828. Me_3SnOMe, solution: Weidlein, J.; Müller, U.; Dehnicke, K. *Schwingungsfrequenzen I*, *Hauptgruppenelemente*; Thieme Verlag: Stuttgart, New York, 1981; p 134. Me_3SnSMe, liquid: Anderson, J. W.; Barker, G. K.; Drake, J. E.; Rodger, M. *J. Chem. Soc., Dalton Trans.* **1973**, 1716. Me_3SnNMe_2, CCl_4 solution: Marchand, A.; Forel, M.-T.; Rivière-Baudet, M. *J. Organomet. Chem.* **1978**, *156*, 341. $MeSnH_3$, gas phase: Kimmel, H.; Dillard, C. R. *Spectrochim. Acta* **1968**, *24A*, 909.

(9) Me_3Sn−Cl/Br/I, Me_3Sn−OEt/S^{n}Bu, Me_3SnNMe_2, Me_4Sn: Harrison, P. G. In *Chemistry of Tin*; Harrison, P. G., Ed.; Blackie: Glasgow, London, 1989; p 13. BE(Sn−F) and BE(Sn−Se) were estimated from the bond dissociation energies of the diatomic molecules FSn and SeSn: Kerr, J. E.; Trotmann-Dickenson, A. F. In *CRC Handbook of Chemistry and Physics*, 63rd ed.; Weast, R. C., Astle, M. J., Eds.; CRC Press: Boca Raton, FL, 1982; p F-185.

(10) Jensovsky, L. *Z. Chem.* **1964**, *4*, 75.

(11) The thermochemical Pauling electronegativity of I is 2.66 and of C is 2.55: Huheey, J. E.; Keiter, E. A.; Keiter, R. L. *Inorganic Chemistry*: *Principles of Structure and Reactivity*, 4th ed.; Harper Collins: New York, 1993; p 187.

Table 3. Stretching Vibrations ν (IR and Raman (cm^{-1}), Intensities in Brackets (Relative Peak Height Intensities)) of the Coordination Polyhedra for Tin in HalMeSn(SCH_2CH_2)$_3$X (Hal = Cl, Br, I, Me; X = O, S, NMe)

		X = O			X = S		
assignmt		**4a** (Hal = Cl)	**4b** (Hal = Br)	**4c** (Hal = I)	**5a** (Hal = Cl)	**8b** (Hal = Br)	**5c** (Hal = I)
$\nu(SnS_2)_{as}$	IR	374 vs (98)	372 vs (95)	367 vs (100)	362 vs (98)	357 vs (100)	357 vs (100)
	Raman	*c*	*c*	*c*	372 m (20)	355 m (29)	354 m (16)
$\nu(SnS_2)_s$	IR	364 vs (93)	364 vs (90)	*c*	337 m (78)	337 s (66)	336 s (41)
	Raman	367 vs (93)	363 vs (100)	354 vs (100)	335 vs (100)	333 vs (100)	336 vs (98)
$\nu(Sn-Me_{eq})$	IR	538 vs (92)	539 vs (80)	536 s (35)	542 vs (100)	532 s (77)	527 s (41)
	Raman	542 s (63)	540 s (65)	545 s (43)	540 s (47)	535 s (50)	528 s (33)
$\nu(Sn-Hal_{ax})$	IR	296 vs,br (100)	203 vs,br (100)	*a*	275 m (82)	190 vs,br (93)	*a*
	Raman	290 s,br (100)	204 s (67)	164 vs (100)	276 s (26)	192 s (50)	134 vs (100)
$\nu(X\cdots Sn)$	IR	*c*	312 m (40)	310 w (12)	*a*	*c*	*a*
	Raman	310 m (14)	308 m (23)	318 m (20)	130 s (26)	130 sh (30)	*d*

		X = NMe			Hal = Me		
assignmt		**6a** (Hal = Cl)	**6b** (Hal = Br)	**6c** (Hal = I)	**7a** (X = O)	**8a** (X = S)	**9a** (X = NMe)
$\nu(SnS_2)_{as}$	IR	380 s (70)	380 vs (100)	378 vs (100)	345 vs (100)	336 vs (100)	359 s (60)
	Raman	378 m (26)	379 s (32)	377 m (19)	*c*	337 w (7)	356 m (11)
$\nu(SnS_2)_s$	IR	341 m (60)	341 s (89)	338 s (89)	*c*	*c*	320 vs (90)
	Raman	334 vs (100)	335 vs (95)	331 s (50)	345 vs (100)	329 vs (100)	323 vs (80)
$\nu(Sn-Me_{eq})$	IR	532 m (55)	522 s (85)	519 vs (96)	536 s (60)	536 vs (95)	512 vs (99)
	Raman	532 vs (94)	525 vs (83)	519 s (33)	538 m (35)	536 m (40)	511 s (56)
$\nu(Sn-Hal_{ax})$	IR	258 vs (100)	*a*	*a*	517 s (60)	515 s (87)	498 vs (100)
	Raman	258 m (15)	157 vs (100)	129 vs (100)	518 s (60)	516 vs (99)	498 vs (100)
$\nu(X\cdots Sn)$	IR	*b*	*b*	*c*	321 m (52)	*c*	*b*
	Raman	365 w (11)	*c*	297 m (16)	322 m (18)	*c*	*b*

[a] IR <200 cm^{-1} not measured. [b] Hidden by $\nu(SnS_2)$. [c] No appearance in the experimental spectra. [d] Hidden by ν(Sn−Hal).

$\Delta\nu$ were transformed into exponential Pauling-type bond orders BO (see eq 1) and into force constant differences Δf, respectively. BO and Δf were arranged in sequences. On the basis of these sequences, the control of the HOMO's and LUMO's of the path was discussed.[1]

Distance Data. To set the occupied MO's of the path on a semiquantitative energy scale, BO and $\Delta\nu$ are referenced in Tables 4−7 to standard single-bond energies BE(std). Concerning the bond orders BO, the transformation into energy values is straightforward in terms of the familiar Morse function (eq 2a).[6] The

$$\Delta BE = -BE(std)(1 - BO)^2 \quad \Delta BE(dist) \qquad (2a)$$

$$BO > 1: \ \Delta BE \text{ negative}$$

$$\Delta BE = -BE(std) - [-BE(std)(1 - BO)^2] \quad \Delta BE(dist)\text{-HOMO} \qquad (2b)$$

differences ΔBE are deviations from the tetrahedral sp^3-hybridized MO's. With regard to the three-center HOMO $^3\sigma(n)$, the energy of the reference is the zero energy of the nonbonded donor, and eq 2a transforms into eq 2b.

Vibrational Data. With regard to the wavenumber shift $\Delta\nu$ between the assigned wavenumber and a single-bond wavenumber standard ν(std), a problem arises in deriving the electronic energy from the vibrational energy. The eqs 3a,b give an attempt to solve

$$\frac{\Delta BE}{BE(std)} = \left(\frac{|\Delta\nu|}{\nu(std)}\right)^{1.85} \quad \Delta BE(vib) \qquad (3a)$$

$$\Delta\nu \text{ negative: } \Delta BE \text{ positive}$$

$$\frac{\Delta BE}{BE(std)} = 0.6 - \left(\frac{|\Delta\nu|}{\nu(std)}\right)^{1.85} \quad \Delta BE(vib)\text{-HOMO} \qquad (3b)$$

the problem by the use of a kind of Morse function. The exponent 1.85 is adjusted in such a manner that the ΔBE values from the vibrational data have generally the same order of magnitude as the ΔBE values from the distance data.

Figures 3 and 4 show the results derived from the bond distances (bond order given above each MO) for the pentacoordinate compounds with oxygen donors (series **2** top, series **4** bottom) and for the heptacoordinate compounds (**8a**, three donor S atoms; series **9**,[3c] three donor O atoms). The latter compounds have one equatorial ligand and three axial three-center interactions X···Sn−R(ax).

Total Energy Gain. The single values of ΔBE for each MO (arrows in Figures 3 and 4) are added up to give $\Sigma_{eq}\Delta BE$ and $\Sigma_{ax}\Delta BE$. The latter is added up to give the total energy gain $\Sigma\Delta BE$ of the occupied MO's. The total energy gain, as derived from the bond order calculations (energy coordinate), is plotted in Figure 5 versus the configurational coordinate $\Delta\Sigma(\theta)$. Since no bond length data are available for compounds **1**, **6**, and **5c**, the sums derived from the vibrational data have been used. The total energy gains are given at the left border of Figure 5. Due to the assumptions made (eq 3 and footnote *f* in Table 5), their accuracy should be considered as poor in comparison with the values obtained from the distance data. Obviously, the scaling of both derived energy sets—from the distance data and from the vibrational data—differs. Hence, in Figure 5, comparisons should be done only within each group.

LUMO and Movable Charge. The LUMO $^3\sigma^*$ of each three-center interaction is located above the occupied orbitals in Figures 3 and 4, and it is delocalized over the total pentacoordinate bonding scheme. This LUMO is important due to its influence on the total energy of the path in addition to the energies of the occupied MO's. Its activity arises because of its population with a movable charge given by the axial ligand R(ax) and also by the equatorial ligands R′(eq) and two S(eq) into the path. The movable charge originates from the lone pairs of the halides and of the chalcogenides,

Table 4. Energy Scaling of the Path from a Tetrahedron to a Trigonal Bipyramid in Terms of Structural and Vibrational Data for the Compounds with Donor Oxygen (Series 2 and 4 and Compound 7a)

entry[a]									
type	bond	position	**2a** (Cl_2)	**2b** (Br_2)	**2c** (I_2)	**4a** (R = Cl, R′ = Me)	**4b** (R = Br, R′ = Me)	**4c** (R = I, R′ = Me)	**7a** (Me_2)
					Bond Length Data ("dist")				
d, Å	Sn−S[b]	eq	2.369(3)	2.361(3)	2.381(2)	2.38(1)	2.393(2)	2.393(1)	2.405(1)
Δ*d*, Å			−0.03	−0.04	−0.02	−0.02	−0.01	−0.01	0.01
BO			1.10	1.14	1.07	1.07	1.03	1.03	0.97
ΔBE, kJ/mol			−2	−4	−1	−1	0	0	0
d, Å	Sn−R′	eq	2.346(3)	2.477(2)	2.682(1)	2.17(4)	2.126(7)	2.143(6)	2.119(7)
Δ*d*, Å			−0.01	−0.02	−0.03	0.02	−0.02	−0.01	−0.03
BO			1.03	1.07	1.10	0.94	1.07	1.03	1.10
ΔBE, kJ/mol			0	−1	−2	1	−1	0	−2
d, Å	Sn···O	ax	2.359(6)	2.41(1)	2.431(5)	2.42(2)	2.440(4)	2.466(3)	2.774(5)
Δ*d*, Å			0.36	0.41	0.43	0.44	0.44	0.47	0.77
BO			0.31	0.27	0.25	0.26	0.24	0.22	0.08
ΔBE, kJ/mol			−144	−128	−120	−122	−116	−108	−42
d, Å	Sn−R	ax	2.376(3)	2.536(2)	2.738(1)	2.413(1)	2.561(1)	2.762(1)	2.133(8)
Δ*d*, Å			0.02	0.04	0.03	0.05	0.06	0.05	−0.02
BO			0.94	0.88	0.91	0.85	0.82	0.85	1.07
ΔBE, kJ/mol			1	4	2	9	8	4	−1
					Vibrational Data ("vib")				
ν, cm^{-1}	Sn−S[c]	eq	383	377	367	370	368	365	345
$\Delta\nu$, cm^{-1}			43	37	27	30	28	15	5
ΔBE, kJ/mol			−5	−4	−2	−2	−2	−1	0
ν, cm^{-1}	Sn−R′	eq	348	243	206	540	539	540	537
$\Delta\nu$, cm^{-1}			17	9	16	13	12	13	10
ΔBE, kJ/mol			−1	−1	−2	0	0	0	0
ν, cm^{-1}	Sn···O	ax	306	305	307	310	310	314	322
$\Delta\nu$, cm^{-1}			−225	−226	−224	−221	−221	−217	−209
ΔBE, kJ/mol			−109	−108	−109	−111	−111	−113	−116
ν, cm^{-1}	Sn−R	ax	324	208	168	293	204	164	518
$\Delta\nu$, cm^{-1}			−7	−26	−21	−38	−30	−25	−13
ΔBE, kJ/mol			0	4	3	6	6	5	0
					Sums of Gain of Energy				
Σ_{eq}ΔBE(dist), kJ/mol			−4	−9	−4	−1	−1	0	−2
Σ_{ax}ΔBE(dist), kJ/mol			−143	−124	−128	−112	−108	−104	−43
ΣΔBE(dist), kJ/mol			−147	−133	−132	−113	−109	−104	−45
Σ_{eq}ΔBE(vib), kJ/mol			−11	−9	−6	−4	−4	−2	0
Σ_{ax}ΔBE(vib), kJ/mol			−109	−104	−106	−105	−105	−107	−116
ΣΔBE(vib), kJ/mol			−120	−113	−112	−109	−109	−109	−116
					Bond Angle Data ("Goodness of a Trigonal Bipyramid")				
Δ$\Sigma(\sigma)$, deg[d]			61	59	51	58	56	53	37
ΔSn(plane), Å			0.29	0.29	0.36	0.32	0.33	0.36	0.57

[a] As single-bond standards, the following values were chosen. Distances d(Sn−F/Cl/Br/I) = 1.95/2.36/2.50/2.71 Å, *d*(Sn−O/S/Se) = 2.00/2.40/2.55 Å, *d*(Sn−N) = 2.09 Å, *d*(Sn−C) = 2.15 Å.[7] Wavenumbers ν(Sn−F/Cl/Br/I) = 588/331/234/189 cm^{-1}, ν(Sn−O/S/Se) = 531/340/237 cm^{-1}, ν(Sn−N) = 618 cm^{-1}, ν(Sn−C) = 527 cm^{-1}.[8] Bond energies BE(Sn−F/Cl/Br/I) = −360/−315/−255/−190 kJ/mol, BE(Sn−O/S/Se) = −275/−215/−195 kJ/mol, BE(Sn−N) = −170 kJ/mol, BE(Sn−C) = −200 kJ/mol.[9] The Pauling-type bond orders BO were calculated according to eq 1. The bond energy differences ΔBE were calculated according to eqs 2 and 3. For further details of the entry description see ref 1. [b] Average. [c] Average ("mittelfrequenz" of ν_{as} and ν_s).[10] [d] Tetrahedron = 0°. Trigonal bipyramid (sum of equatorial−equatorial angles = 3 × 120°) − (sum of axial−equatorial angles = 3 × 90°) = 90°.[5b]

from the so-called hyperconjugation of methyl,[12a] or, in the case of aromatic ligands, from their π-electron systems. The calculation of ΣΔBE from the bond distances of the compounds Cl−(Ph)Sn(SCH_2CH_2)$_2$X (X = O, S)[13] gives −119 and −80 kJ/mol, respectively. These energy gains are located in Figure 5 between **2** and **4** or between **3** and **5**, respectively. It can be stated that tin(IV) has the property of π-Lewis acidity in addition to its σ-Lewis acidity.

The single energies of the occupied MO's, determined by means of eqs 2 and 3, and also the partial sums should be corrected for these influences of π-Lewis acidity. In the total energy gain ΣΔBE the different corrections are balanced out. It can be regarded as a true semiquantitative figure. The other non-LUMO-corrected data indicate only relative trends, and the important question about the energetic position of the LUMO is now raised.

Two cases are possible. First, as was assumed in ref 1, the LUMO $^3\sigma^*$ is located in the antibonding region, and it destabilizes the pentacoordinate bonding scheme. Second, the LUMO $^3Q^*$ is located in the bonding region. A choice between these two possibilities is the basis of this study.

π-Lewis Acidity versus Electronegativity. If the discussion is first restricted to the halides as ligands, it is unambiguous that both the charge-donating power into the LUMO $^3\sigma^*$ and also the charge-withdrawing power within the bonding orbital $^3\sigma$(Sn−Hal) (electronegativity) decrease in the order Cl > Br > I. In addition, it is clear from ref 1 that in most cases the electronegative chlorine ligand favors hypervalency the

(12) (a) March, J. *Advanced Organic Chemistry: Reactions, Mechanisms, and Structure*, 3rd ed.; Wiley: New York, 1985; p 64. (b) pp 16, 32. (c) p 255.

(13) Dräger, M. *Z. Naturforsch.* **1981**, *36B*, 437; *Z. Anorg. Allg. Chem.* **1985**, *527*, 169.

Table 5. Energy Scaling of the Path from a Tetrahedron to a Trigonal Bipyramid in Terms of Structural and Vibrational Data for the Compounds with Donor Sulfur (Series 3 and Compounds 5a,b) and Donor NMe (Compound 9a)

entry[a]			X = S					
type	bond	position	**3a** (Cl_2)	**3b** (Br_2)	**3c** (I_2)	**5a** (R = Cl, R′ = Me)	**5b** (R = Br, R′ = Me)	X = NMe **9a** (Me_2)
			Bond Length Data ("dist")					
d, Å	Sn−S[b]	eq	2.387(3)	2.400(2)	2.397(2)	2.405(1)	2.408(2)	2.428(1)
Δ*d*, Å			−0.01	0	0	0.01	0.01	0.03
BO			1.03	1.00	1.00	0.97	0.97	0.91
ΔBE, kJ/mol			0	0	0	0	0	2
d	Sn−R′	eq	2.348(3)	2.49(1)	2.700(1)	2.122(3)	2.138(6)	2.14(1)
Δ*d*			−0.01	−0.01	−0.01	−0.03	−0.01	−0.01
BO			1.03	1.03	1.03	1.10	1.03	1.03
ΔBE, kJ/mol			0	0	0	2	0	0
d, Å	Sn···X	ax	2.760(3)	2.767(2)	2.779(2)	2.863(1)	2.835(2)	2.566(5)
Δd, Å			0.36	0.37	0.38	0.46	0.44	0.48
BO			0.31	0.30	0.29	0.22	0.24	0.21
ΔBE, kJ/mol			−113	−110	−107	−84	−91	−64
d, Å	Sn−R	ax	2.392(3)	2.545(1)	2.786(1)	2.444(1)	2.582(1)	2.16(1)
Δd, Å			0.03	0.05	0.08	0.08	0.08	0.01
BO			0.91	0.85	0.77	0.77	0.77	0.97
ΔBE, kJ/mol			3	6	10	17	13	0
			Vibrational Data ("vib")					
ν, cm^{-1}	Sn−S[c]	eq	353	353	*e*	352	346	340
$\Delta\nu$, cm^{-1}			13	13		12	6	0
ΔBE, kJ/mol			0	−1		−1	0	0
ν, cm^{-1}	Sn−R′	eq	351	239	*e*	541	533	511
$\Delta\nu$, cm^{-1}			20	5		14	6	16
ΔBE, kJ/mol			−2	0		0	0	0
ν, cm^{-1}	Sn···X	ax	134	128	*e*	130	130	(360)[f]
$\Delta\nu$, cm^{-1}			−206	−212		−210	−210	−136
ΔBE, kJ/mol			−44	−39		−41	−41	−68
ν, cm^{-1}	Sn−R	ax	311	208	*e*	276	191	498
$\Delta\nu$, cm^{-1}			−20	−26		−55	−48	−29
ΔBE, kJ/mol			2	4		11	14	1
			Sums of Gain of Energy					
Σ_{eq}ΔBE(dist), kJ/mol			0	0	0	2	0	4
Σ_{ax}ΔBE(dist), kJ/mol			−110	−104	−97	−67	−78	−64
ΣΔBE(dist), kJ/mol			−110	−104	−97	−65	−78	−60
Σ_{eq}ΔBE(vib), kJ/mol			−2	−2		−2	0	0
Σ_{ax}ΔBE(vib), kJ/mol			−42	−35		−30	−27	−67
ΣΔBE(vib), kJ/mol			−44	−37		−32	−27	−67
			Bond Angle Data ("Goodness of a Trigonal Bipyramid")					
ΔΣ(σ), deg[d]			70	70	70	72	73	55
ΔSn(plane), Å			0.21	0.21	0.21	0.19	0.18	0.34

[a] See footnote *a* in Table 4. [b] Average. [c] Average ("mittelfrequenz"[10] of ν_{as} and ν_s). [d] See footnote *d* in Table 4. [e] No reliable vibrational data; compound decomposes. [f] Transition hidden by ν(Sn−S)$_{as}$. Value estimated by using ν(Sn−N) in the series of compounds F/Cl/Br/I−Sn($CH_2CH_2CH_2$)$_3$N.[1]

least. In eight different series of compounds, the maximum hypervalency usually exists between bromine and iodine. The two factors of electronegativity and π-Lewis acidity are counteractive and balance each other out. One of the two factors stabilizes the hypervalency, and the other one destablizes it. In conformity with all previous reports,[2,3] the electronegativity was chosen as the stabilizing factor in ref 1.

In this study, methyl has been included as an additional ligand. With regard to the π-donor strength, the order Cl > Br > I ≫ Me holds, whereas with regard to the electronegativity, the order Cl > Br > I ≈ Me[11] exists. Experimentally, all compounds with R′(eq) = Hal are in the same range of hypervalency. If R′(eq) = Me is introduced, a distinct decrease of hypervalency occurs which is followed by an even more distinct decrease if also R(ax) is altered to methyl. This result corresponds better with the order of the π-donor strength than with the order of the electronegativity. In addition, in Figure 3 an enhanced electronegativity of the axial ligands increases their MO's (full line) above the starting values of their sp^3 bond energies (dotted line), and a loss of energy results.

Both results suggest the assumption that the LUMO $^3\sigma^*$ is located in the bonding region and that its population with charge is the actual drive for hypervalency. On the other hand, the counteracting electronegativity of the ligands destabilizes the pentacoordinate bonding system. Generally considered, the counteracting of electronegativity and movable charge is by no means unusual. It is simply a special case of one of the most familiar phenomena of organic chemistry, the mutual interaction between the inductive and the mesomeric effect.[12b]

Heptacoordination. The three three-center bonds of the heptacoordinate compounds **8a** and **10** in Figure 4 can be discussed in the same manner as above. The configurational coordinate would be analogous to the case in Figure 5, the "goodness" of a monocapped octahedron.

Table 6. Energy Scaling of the Path from a Tetrahedron to a Trigonal Bipyramid in Terms of Vibrational Data for the Compounds with Donor NMe (Series 1 and 6) and Compound 5c

entry[a]			X = NMe						X = S
type	bond	position	**1a** (Cl_2)	**1b** (Br_2)	**1c** (I_2)	**6a** (R = Cl, R′ = Me)	**6b** (R = Br, R′ = Me)	**6c** (R = I, R′ = Me)	**5c** (R = I, R′ = Me)
					Vibrational Data ("vib")				
ν, cm^{-1}	Sn−S[c]	eq	366	362	355	358	359	356	346
$\Delta\nu$, cm^{-1}			26	42	15	18	19	16	6
ΔBE, kJ/mol			−2	−5	−1	−1	−1	−1	0
ν, cm^{-1}	Sn−R′	eq	325	228	172	532	523	519	527
$\Delta\nu$, cm^{-1}			−6	−6	−17	5	−4	−8	0
ΔBE, kJ/mol			0	0	2	0	0	0	0
ν, cm^{-1}	Sn···X	ax	(380)[c]	(380)[c]	(380)[c]	365	(331)[e]	297	(130)[d]
$\Delta\nu$, cm^{-1}			−238	−238	−238	−253	−287	−321	−210
ΔBE, kJ/mol			−73	−73	−73	−69	−61	−51	−41
ν, cm^{-1}	Sn−R	ax	294	163	140	258	157	129	134
$\Delta\nu$, cm^{-1}			−37	−71	−49	−73	−77	−60	−55
ΔBE, kJ/mol			6	28	16	19	33	23	19
					Sums of Gain of Energy				
Σ_{eq}ΔBE(vib), kJ/mol			−4	−10	0	−2	−2	−2	0
Σ_{ax}ΔBE(vib), kJ/mol			−67	−45	−57	−50	−28	−28	−22
ΣΔBE(vib), kJ/mol			−71	−55	−57	−52	−30	−30	−22

[a] See footnote *a* in Table 4. [b] Average ("mittelfrequenz"[10] of ν_{as} and ν_s). [c] See footnote *f* in Table 5. [d] Transition hidden by ν(Sn−Hal). Value estimated by using ν(Sn···S) in the compounds **5a**,**b**. [e] Transition hidden by $\nu(SnS_2)_s$. Value estimated as average of ν(Sn···N) in **6a**,**c**.

Table 7. Energy Scaling of the Path from a Tetrahedron to a Monocapped Octahedron in Terms of Structural Data for the Heptacoordinate Compounds 8a and 10[a]

entry[b]			X = 3 S	X = 3 O			
type	bond	position	**8a** (R = 2 S, Me)	**10a** (R = 3 Cl)	**10a′** (R = 3 Cl)	**10b** (R = 3 Br)	**10d** (R = 3 F)
				Bond Length Data ("dist")			
d, Å	Sn−C	"eq"	2.134(3)	2.249(9)	2.265(9)	2.312(5)	2.22(1)
Δd, Å			−0.02	0.1	0.12	0.16	0.07
BO			1.07	0.72	0.68	0.60	0.79
ΔBE, kJ/mol			−1	16	20	32	9
d, Å	Sn···X		3.514(1)	2.555(7)	2.603(7)	2.595(3)	2.454(7)
Δd, Å			1.11	0.56	0.60	0.59	0.45
BO			0.03	0.17	0.14	0.15	0.23
ΔBE, kJ/mol			−13	−86	−72	−76	−112
d, Å	Sn−R		2.147(3)	2.400(3)	2.377(3)	2.511(1)	1.956(6)
Δd, Å			0	0.04	0.02	0.01	0.01
BO			1.00	0.88	0.94	0.97	0.97
ΔBE, kJ/mol			0	5	1	0	0
d, Å	Sn···X		3.678(2)	2.640(7)	2.576(7)	2.606(4)	2.455(8)
Δd, Å			1.28	0.64	0.58	0.61	0.46
BO			0.07	0.13	0.15	0.14	0.23
ΔBE, kJ/mol			−29	−67	−76	−72	−112
d, Å	Sn−R		2.435(1)	2.374(3)	2.393(2)	2.532(1)	1.948(7)
Δd, Å			0.04	0.01	0.03	0.03	0
BO			0.88	0.97	0.91	0.91	1.00
ΔBE, kJ/mol			3	0	3	2	0
d, Å	Sn···X		4.097(2)	2.593(7)	2.611(7)	2.760(4)	2.399(7)
Δd, Å			1.70	0.59	0.61	0.76	0.40
BO			0.03	0.15	0.14	0.09	0.28
ΔBE, kJ/mol			−13	−76	−72	−47	−132
d, Å	Sn−R		2.435(1)	2.390(3)	2.386(3)	2.543(1)	1.975(6)
Δd, Å			0.04	0.03	0.03	0.04	0.03
BO			0.88	0.91	0.91	0.88	0.91
ΔBE, kJ/mol			3	3	3	4	3
				Sums of Gain of Energy ("dist")			
Σ_{eq}ΔBE, kJ/mol			−1	16	20	32	9
Σ_{ax}ΔBE, kJ/mol			−49	−227	−213	−189	−353
ΣΔBE, kJ/mol			−50	−211	−193	−157	−342
				Bond Angle Data ("Goodness of a Monocapped Octahedron")			
$\Delta\Sigma(\theta)$, deg[c]			27	76	74	69	85

[a] Data taken from ref 3c. [b] See footnote *a* in Table 4. [c] Tetrahedron = 0°. Monocapped octahedron (sum of angles between 3- and 4-fold axes = 3 × 125.27°) − (sum of angles between 4-fold axes = 3 × 90°) = 106°.

Hypervalency for the Group 14 Elements. It has long been known that hypervalency of silicon is restricted to some special cases, for which the number of known compounds has grown rapidly over the last 10 years.[14,15] Little has been cited in the literature concerning the hypervalency of germanium,[14,16] despite the fact that germanium exhibits a greater hypervalency than silicon.[17]

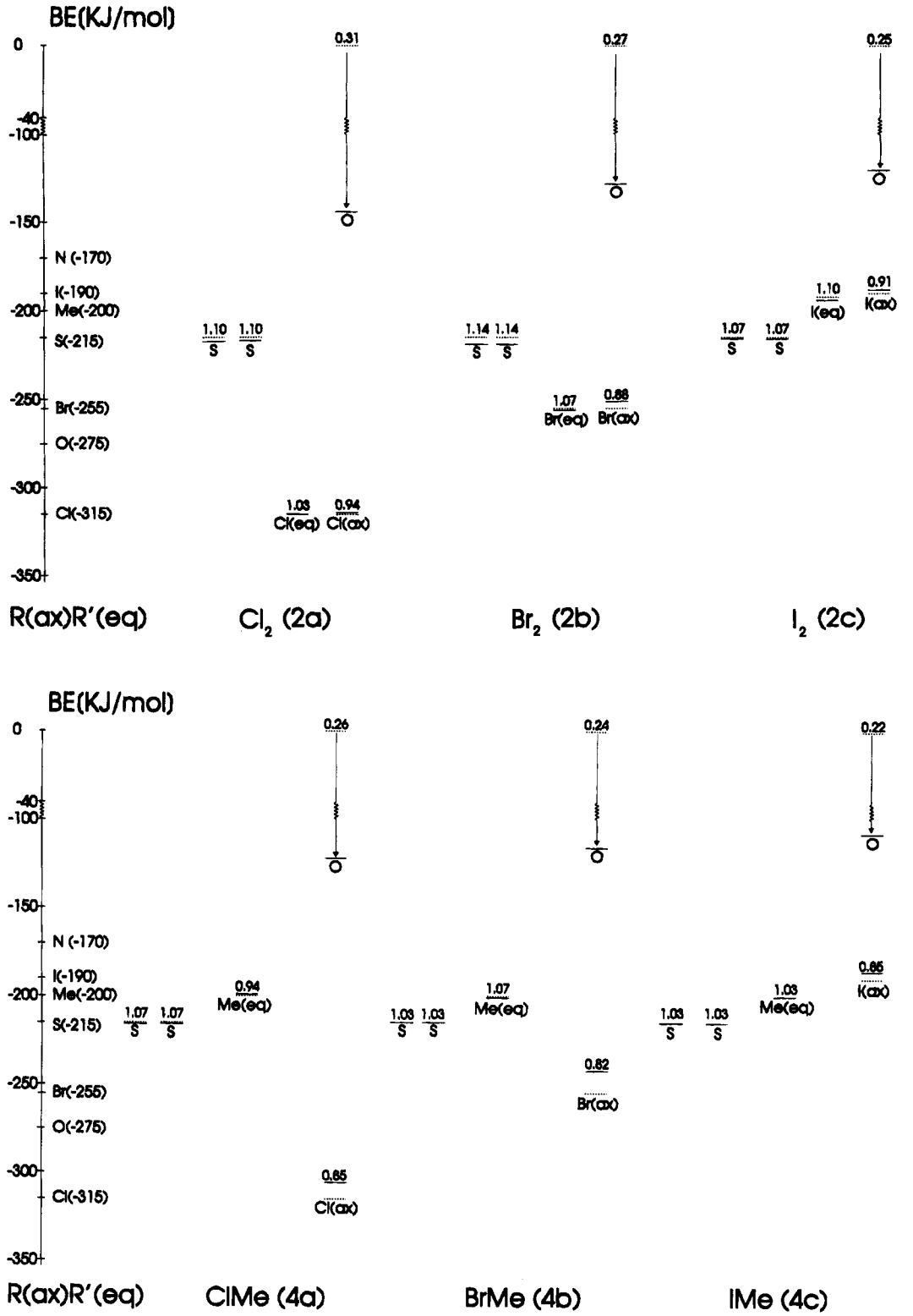

Figure 3. Semiquantitative diagrams of the five occupied molecular orbitals around Sn in the compounds **2** (top) and **4** (bottom): (dotted lines) starting values of a nonbonded donor (bond energy BE = 0) and of a tetrahedral configuration; (solid lines) energy values from the bond elongations and contractions on the path to a trigonal bipyramid (Table 4). The numerical value above each MO is the Pauling-type bond order.

Hypervalency is normal in the case of lead, rather than the tetrahedral coordination.[14,18] With regard to the arguments given above, the LUMO $^3\sigma^*$ of the three-center interaction is higher for silicon and germanium than for tin and appreciably lower for lead. The progressive lowering of the LUMO as one descends the group 14 column and the marked drop for lead can be accounted for in terms of the relativistic effect.[19]

Nucleophilic Attack. Any discussion of the broad subject of bimolecular nucleophilic attack at tetrahedral carbon[12c] and silicon[20] shall be omitted in this study. It shall only be mentioned that the model given presents an explanation for the enhanced reaction rate of pentacoordinate silicon with nucleophiles.[21] The discussed low-lying LUMO of hypervalency offers a preferred site of attack.

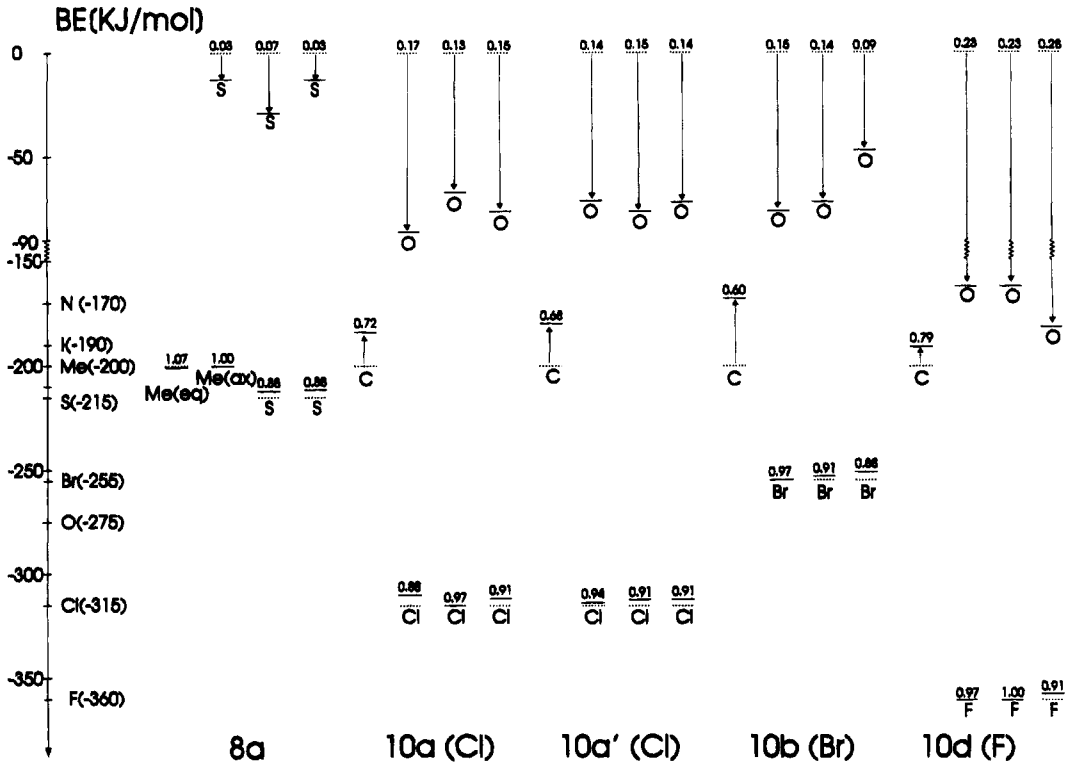

Figure 4. Semiquantitative diagram of the seven occupied molecular orbitals around Sn in the compounds **8a** and **10**: (dotted lines) starting values of the three nonbonded donors (bond energies BE = 0) and of a tetrahedral configuration; (solid lines) energy values from the bond elongations and contractions on the path to a monocapped octahedron (Table 7). The numerical value above each MO is the Pauling-type bond order.

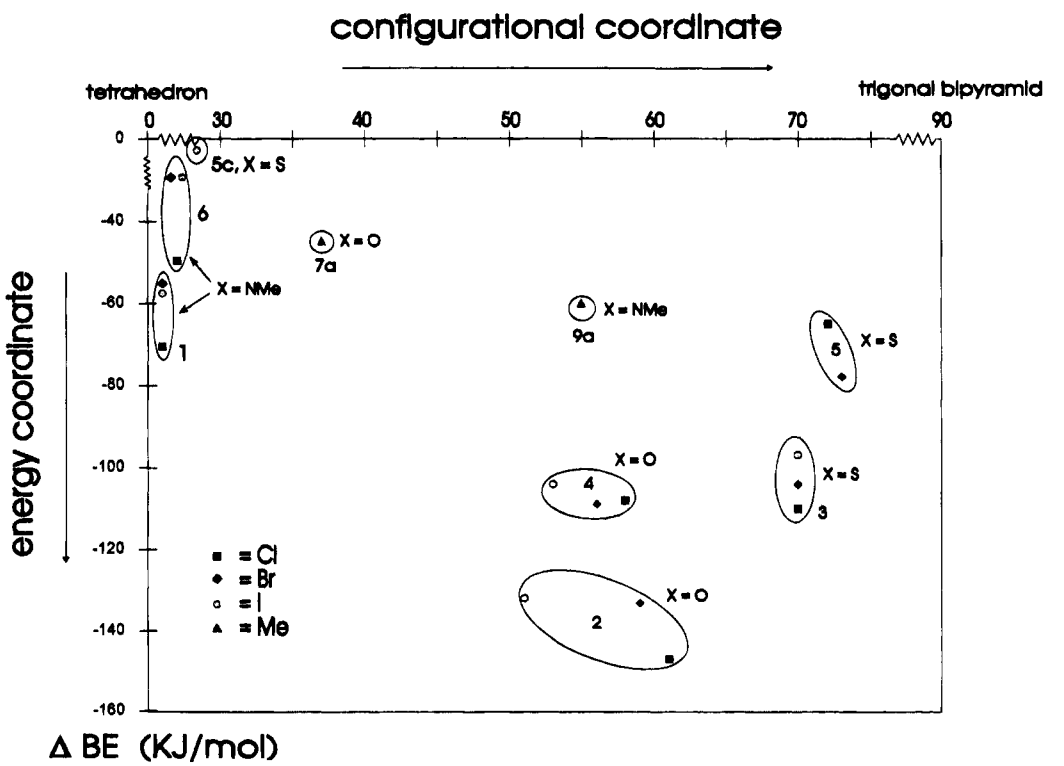

Figure 5. Plot of the total energy gain (energy coordinate) versus the goodness of a trigonal bipyramid (configurational coordinate $\Delta\Sigma(\theta)$, deg) for the compounds **2**–**5**, **7a**, and **9a** (Tables 4 and 5). The related energy values for the compounds **1**, **6**, and **5c** from the vibrational data are given at the left border (Table 6; no configurational coordinate available).

Experimental Section

Syntheses. The methylhalogenostannocanes and the dimethylstannocanes were prepared by heating the respective methyltin halide with the respective disodium dithiolate in ethanol for several hours.[22] A representative detailed procedure follows for the compound **6a**. To a solution of 10 mmol of $NMe(CH_2CH_2SH)_2$[1] in 100 mL of ethanol is added 0.46 g (20 mmol) of sodium. The reaction mixture is refluxed for 1 h. To the boiling reaction mixture is added a solution of 10

Table 8. Details of Preparation and Analytical Data of the Methylhalogenostannocanes and Dimethylstannocanes

compd	amt of $Me_{4-n}SnCl_n$ (mmol)/solvent (amt (cm^3))[a]	amt of ligand (mmol)/solvent (amt (cm^3))	time (h)	yield (%)	formula	M_r	*m/e* (%)	color	mp (°C)	anal. found (calcd) C	H	S	N	Hal
4a	21/ethanol (100)	21/ethanol (50)	4	55	$C_5H_{11}ClOS_2Sn$	305.43	306 (20)	colorless	140−141	19.98 (19.66)	3.67 (3.63)	21.40 (20.99)		*c*
5a	21/ethanol (100)	21/ethanol (50)	4	30	$C_5H_{11}ClS_3Sn$	321.49		colorless	149	19.00 (18.68)	3.51 (3.45)	30.36 (29.92)		*c*
6a	10/toluene (100)	10/ethanol (100)	4	57	$C_6H_{14}ClNS_2Sn$	318.47	304[d] (84)	colorless	246[e]	22.65 (22.63)	4.58 (4.43)	19.53 (20.13)	4.49 (4.40)	11.17 (11.13)
4b	13/ethanol−benzene 1:1 (120)	13/ethanol (80)	5	64	$C_5H_{11}BrOS_2Sn$	349.87	350 (26)	colorless	171	17.35 (17.16)	3.17 (3.17)	18.50 (18.33)		*c*
5b	13/ethanol (150)	13/ethanol (80)	5	50	$C_5H_{11}BrS_3Sn$	365.93	351[d] (65)	colorless	143−144	16.88 (16.41)	2.49 (3.03)	26.63 (26.28)		*c*
6b	10/toluene (100)	10/ethanol (100)	4	40	$C_6H_{14}BrNS_2Sn$	362.92	349[d] (95)	colorless	233[e]	20.34 (19.86)	4.28 (3.89)	16.79 (17.67)	3.67 (3.86)	22.06 (22.02)
4c	4/ethanol−benzene 3:1 (200)	4/ethanol (50)	4	50	$C_5H_{11}IOS_2Sn$	396.87		light yellow	153	15.05 (15.13)	2.60 (2.79)	16.33 (16.16)		*c*
5c	4/ethanol−benzene 3:1 (200)	4/ethanol (50)	4.5	50	$C_5H_{11}IS_3Sn$	412.93	398[d] (4)	light yellow	147	14.58 (14.54)	2.71 (2.69)	23.48 (23.29)		*c*
6c	10/ethanol (100)	10/ethanol (100)	4	24	$C_6H_{14}INS_2Sn$	409.92	396[d] (6)	light yellow	208[e]	17.13 (17.58)	3.44 (3.44)	14.65 (15.64)	3.03 (3.42)	34.60 (30.96)
7a	23/ethanol−benzene 1:1 (100)	23/ethanol (50)	5	66	$C_6H_{14}OS_2Sn$	285.01	286 (38)	colorless	50	25.30 (25.29)	5.03 (4.95)	22.81 (22.50)		
8a	23/benzene (90)	23/ethanol (20)	5	37	$C_6H_{14}S_3Sn$	301.07	287[d] (26)	colorless	72−73	24.01 (23.94)	4.86 (4.69)	31.01 (31.95)		
9a[b]	10/toluene (100)	10/ethanol (100)	4	63	$C_7H_{17}NS_2Sn$	298.05	284[d] (100)	colorless	66	28.03 (28.21)	5.15 (5.75)	21.81 (21.51)	4.73 (4.70)	

[a] $n = 3$ for the compounds **4−6**. $n = 2$ for **7a**, **8a**, and **9a**. [b] Reference 5a. The given results are obtained in this study. [c] Hal not determined. [d] $M^+ - CH_3$. [e] Decomposition.

Table 9. Crystallographic Data for $ClMeSn(SCH_2CH_2)_2O$ (4a), $BrMeSn(SCH_2CH_2)_2O$ (4b), $IMeSn(SCH_2CH_2)_2O$ (4c), and $Me_2Sn(SCH_2CH_2)_2O$ (7a) and Structure Determination Details

	4a	4b	4c	7a
	Crystal Data (Mo Kα$_1$, $\lambda = 0.709\,26$ Å)			
formula, M_r	$C_5H_{11}ClOS_2Sn$, 305.44	$C_5H_{11}BrOS_2Sn$, 349.89	$C_5H_{11}IOS_2Sn$, 396.89	$C_6H_{14}OS_2Sn$, 285.02
cryst habit, color	long hexagonal needle	unregular square block	thin plate	big hexagonal block, colorless
face indices (dist from a common origin inside the cryst (mm))	100; −1,0,0 (0.1) 010; 0,−1,0 (0.1) 001, 0,0,−1 (1.0) 110, −1,−1,0 (0.1)	100; −1,0,0 (0.21) 010; 0,−1,0 (0.15) 001; 0,0,−1 (0.18)	100; −1,0,0 (0.3) 010; 0,−1,0 (0.04) 001; 0,0,−1 (0.24)	010; 0,−1,0 (0.036) 001; 0,0,−1 (0.065) −1,0,1; 1,0,−1 (0.63) 101; −1,0,−1 (0.063)
cryst syst, space group	hexagonal, $P6_5$ (No. 169)	monoclinic $P2_1/n$ (No. 14)	monoclinic $P2_1/n$ (No. 14)	orthorhombic; *Pnma* (No. 62)
unit cell dimens				
a (Å)	7.7483(6)	6.9095(6)	7.101(1)	7.306(1)
b (Å), β (deg)	7.7483(6)	14.747(1), 105.87(1)	15.054(1), 107.05(1)	11.601(1)
c (Å)	30.605(3)	10.919(2)	10.939(1)	12.407(1)
least-squares fit	15 rflns, $\theta = 25-32°$	75 rflns, $\theta = 23-26°$	50 rflns, $\theta = 27-29°$	41 rflns, $\theta = 25-32°$
packing; V (Å^3), Z, $F(000)$	1591(1), 6, 888	1070(1), 4, 664	1118(1), 4, 736	1052(2), 4, 560
D_{calcd}, D_{exptl} (g cm^{-3})	1.912, 1.970	2.172, 2.176	2.358, 2.289	1.800, 1.770
	Intensity Data Collection (Mo Kα, $\lambda = 0.710\,69$ Å, graphite monochromator)			
temp (°C), θ range (deg)	23, 0−20	23, 1.5−30	22, 1−30	23, 1−35
$(\sin\theta)_{max}/\lambda$ (Å^{-1})	0.4813	0.7035	0.7035	0.8071
range of *hkl*	+11,+11,+46	+9,+20,±15	+9,+20,±15	+11,+20,+18
ref rflns	3, every 5000 s	3, every 4000 s	3, every 4000 s	3, every 5000 s
loss of intens (%) (time (days))	10 (2)	1 (3)	10 (3)	5 (3)
corr	spline (Tol = 15)	linear	spline (Tol = 10)	spline (Tol = 15)
no. of rflns meas, indep (int R)	2341, 1950 (0.024)	3460, 2763 (0.0388)	3606, 3239 (0.0169)	2636, 2389
no. of rflns used, limit	1497, with $I > 2\sigma(I)$	2262, with $I > 2\sigma(I)$	2855, with $I > 2\sigma(I)$	2117, with $I > 3\sigma(I)$
μ (cm^{-1}), abs cor	27.8, by face indices	61.89, by face indices	51.50, by face indices	25.66, by face indices
range of transmissn	0.7019−0.5318	0.2377−0.1505	0.6628−0.1455	0.2142−0.1129
		Refinement		
choice of thermal params	Sn, Cl, S, C anisotropic; disordered C isotropic; H isotropic fixed	Sn, Br, S, C anisotropic; H isotropic fixed	Sn, I, S, C anisotropic; H isotropic fixed	Sn, S, C anisotropic; H isotropic fixed
no. of variables, ratio rflns/var	93, 16	94, 24	94, 30	66, 32
last shifts	<0.002σ	<0.001σ	<0.003σ	<0.002σ
final R, R_w	0.0587, 0.2526[a]	0.0426, 0.0605	0.0422, 0.0764	0.0564, 0.1075
enantiomorphism (signif >99.5%)	$R_w(2)/R_w(1) = 1.011$			
weighting scheme w^{-1}	$\sigma^2(F^2) - 0.1007P^2 + 7.8340P$[b]	$\sigma^2(F) + 0.002248F^2$	$\sigma^2(F) + 0.012987F^2$	$\sigma^2(F) + 0.007510F^2$
final diff Fourier maxima (e Å^{-3})	1.5 (near Sn)	2.3 (near Sn)	1.0 (near I)	3.5 (near Sn)

[a] R according to SHELX-76; R_w according to SHELX-93, value higher than R_w according to SHELX-76, due to the use of intensities in the refinement. [b] $P = {}^1/_3((\max F_o; 0) + 2F_c^2)$.

mmol of $MeSnCl_3$ in 100 mL of toluene dropwise with stirring, and the refluxing is continued for 4 h. The mixture is filtered to remove the formed NaCl and cooled. The separated crude product is filtered off and recrystallized from CH_2Cl_2/ether. Table 8 summarizes variations and results for the 12 compounds prepared.

Table 10. Crystallographic Data for $ClMeSn(SCH_2CH_2)_2S$ (5a), $BrMeSn(SCH_2CH_2)_2S$ (5b), and $Me_2Sn(SCH_2CH_2)_2S$ (8a) and Structure Determination Details

	5a	5b	8a
	Crystal Data (Mo Kα$_1$, λ = 0.709 26 Å)		
formula, M_r	$C_5H_{11}ClS_3Sn$, 321.5	$C_5H_{11}BrS_3Sn$, 366.0	$C_6H_{14}S_3Sn_1$, 301.09
cryst habit, color	long plate	long, square needle	irregular square block, colorless
face indices (dist from a common origin inside the cryst (mm))	100; −1,0,0 (0.15) 010; 0,−1,0 (0.06) 001; 0,0,−1 (0.4)	001; 0,0,−1 (0.28) 110; −1,−1,0 (0.05) 1,−1,0; −1,1,0 (0.08)	0,−1,0 (0.18) 1,0,−1 (0.05) 101 (0.1) −1,0,−1 (0.13) −1,0,1 (0.08)
cryst syst, space group	monoclinic, $P2_1/n$ (No. 14)	monoclinic, $P2_1/n$ (No. 14)	monoclinic, $P2_1/n$ (No. 14)
unit cell dimens			
a (Å)	8.907(1)	8.890(3)	10.030(1)
b (Å), β (deg)	13.238(1), 104.78(3)	13.306(6), 104.87(2)	9.904(1), 103.54(3)
c (Å)	9.210(1)	9.356(1)	11.297(1)
least-squares fit	25 rflns, θ = 23−27°	50 rflns, θ = 25−27°	25 rflns, θ = 21−25°
packing: V (Å^3), Z, F(000)	1050(1), 4, 624	1070(1), 4, 696	1091(1), 4, 592
D_{calcd}, D_{exptl} (g cm^{-3})	2.034, 2.060	2.272, 2.288	1.833, 1.800
	Intensity Data Collection (Mo Kα, λ = 0.710 69 Å, graphite monochromator)		
temp (°C), θ range (deg)	20, 1−27.5	20, 1−27.5	20, 1−27.5
sin θ_{max}/λ (Å^{-1})	0.6497	0.6497	0.6497
range of hkl	+11,+17,±11	+11,+17,±12	+12,+13,±14
ref rflns	3, every 3000 s	3, every 5000 s	3, every 5000 s
loss of intens (%) (time (days))	3 (3)	10 (2)	4 (5.5)
cor	linear fit	direct fit	linear fit
refl: meas, indep (int R)	2563, 2416 (0.0332)	2715, 2446 (0.0320)	2635, 2635 (0.0107)
refl used, limit	2133, with $I > 3\sigma(I)$	1977, with $I > 2\sigma(I)$	1974, with $I > 2\sigma(I)$
μ (cm^{-1}), abs cor	29.89, by face indices	63.68, by face indices	26.46, by face indices
range of transmissn	0.7022−0.4272	0.6017−0.3417	0.7559−0.5987
	Refinement		
choice of thermal params	Sn, S, Cl, C anisotropic; H isotropic fixed	Sn, S, Br, C anisotropic; H isotropic fixed	Sn, S, C anisotropic; H isotropic fixed
no. of variables, ratio rflns/var	95, 23	94, 21	95, 21
last shifts	<0.001σ	<0.001σ	<0.001σ
final R, R_w	0.0210, 0.0374	0.0334, 0.0565	0.0188, 0.0228
weighting scheme w^{-1}	$\sigma^2(F) + 0.000420F^2$	$\sigma^2(F) + 0.002045F^2$	$\sigma^2(F) + 0.000000F^2$
final diff Fourier maxima (e Å^{-3})	0.5 (near Sn)	1.2 (near Sn)	0.5 (near Sn)

Table 11. Fractional Atomic Coordinates and Equivalent Isotropic Thermal Parameters for $ClMeSn(SCH_2CH_2)_2O$ (4a), $BrMeSn(SCH_2CH_2)_2O$ (4b), $IMeSn(SCH_2CH_2)_2O$ (4c), and $Me_2Sn(SCH_2CH_2)_2O$ (7a) (Esd's in Parentheses)

4a

atom	x	y	z	U(eq), Å^2 [a]
Sn	0.5042(2)	0.1219(2)	0.0000(0)	0.0495(5)
Cl(ax)	0.689(1)	0.030(1)	1.0489(2)	0.078(3)
Me(eq)	0.664(5)	0.172(6)	0.939(1)	0.11(2)
S(1)	0.1983(9)	−0.1853(9)	1.0050(3)	0.077(3)
C(1)[b]	0.084(8)	−0.145(7)	0.957(1)	0.070(6)[c]
C′(1)[b]	0.028(6)	−0.124(8)	0.977(2)	0.070(6)[c]
C(2)[b]	0.071(4)	0.039(5)	0.963(2)	0.070(6)[c]
C′(2)[b]	0.112(7)	0.031(6)	0.943(2)	0.070(6)[c]
O	0.276(2)	0.203(2)	0.9634(6)	0.066(7)
C(3)	0.255(4)	0.357(4)	0.9852(9)	0.07(1)
C(4)	0.457(5)	0.508(4)	1.0006(9)	0.09(2)
S(2)	0.558(1)	0.407(1)	1.0405(3)	0.080(3)

4b

atom	x	y	z	U(eq), Å^2 [a]
Sn	0.9919(5)	0.11324(2)	0.30072(3)	0.0386(1)
Br(ax)	−0.1465(1)	0.23952(5)	0.31781(8)	0.0702(3)
Me(eq)	0.352(1)	0.1330(5)	0.4608(6)	0.061(2)
S(1)	0.1496(3)	0.1638(1)	0.1035(1)	0.0541(5)
C(1)	0.367(1)	0.0941(5)	0.1050(7)	0.067(3)
C(2)	0.329(1)	−0.0049(5)	0.1236(7)	0.064(3)
O	0.2722(6)	−0.0159(3)	0.2388(4)	0.050(1)
C(3)	0.186(1)	−0.1029(4)	0.2497(8)	0.061(2)
C(4)	0.075(1)	−0.0975(4)	0.3485(7)	0.061(2)
S(2)	−0.1226(2)	−0.0103(1)	0.3069(2)	0.0582(6)

4c

atom	x	y	z	U(eq), Å^2 [a]
Sn	0.10468(4)	0.10927(2)	0.30046(2)	0.0342(1)
I(ax)	−0.15511(6)	0.24241(2)	0.31582(4)	0.0603(2)
Me(eq)	0.3574(8)	0.1257(4)	0.4637(5)	0.058(2)
S(1)	0.1540(2)	0.15706(9)	0.1031(1)	0.0506(4)
C(1)	0.364(1)	0.0838(4)	0.1073(6)	0.067(2)
C(2)	0.326(1)	−0.0082(4)	0.1254(6)	0.064(2)
O	0.2775(5)	−0.0188(2)	0.2424(3)	0.047(1)
C(3)	0.1914(9)	−0.1039(3)	0.2555(6)	0.052(2)
C(4)	0.0821(8)	−0.0975(3)	0.3505(5)	0.048(2)
S(2)	−0.1093(2)	−0.01232(9)	0.3059(1)	0.0510(4)

7a

atom	x	y	z	U(eq), Å^2 [a]
Sn	0.09989(4)	−0.25(0)	0.06899(3)	0.0344(2)
Me(ax)[b]	0.062(1)	−0.228(2)	0.2374(7)	0.062(7)
Me(eq)	−0.146(1)	−0.25(0)	−0.0215(6)	0.048(2)
S(1)	0.2687(2)	−0.0738(1)	0.0465(1)	0.0527(3)
C(1)	0.2535(9)	−0.0502(5)	−0.0982(5)	0.058(2)
C(2)	0.341(1)	−0.1503(7)	−0.1633(5)	0.068(2)
O	0.2434(7)	−0.25(0)	−0.1383(5)	0.054(1)

[a] U(eq) = $^1/_3\sum_i\sum_j U(ij)\, a_i^* a_j^* (\mathbf{a}_i \cdot \mathbf{a}_j)$. [b] Disordered. [c] Isotropic thermal parameter.

Structure Determinations. Single crystals were obtained from ethanol (**4a**), petroleum ether (**8a**, **7a**), and toluene (**4b**,**c**, **5a**,**b**). All attempts to get single crystals of $I-(Me)Sn(SCH_2CH_2)_2S$ (**5c**) and of the compounds **6** failed. Crystal data as well as details of intensity data collections and refinements are given in Tables 9 and 10. The densities were determined by flotation in $CHBr_3/CCl_4$ (**4c**), in polytungstate solution (**4b**, **5b**), or in a solution of $K_2[HgI_4]$ (**4a**, **5a**, **7a**, **8a**). The crystals were fixed by gravity and sealed in glass capillaries. The quality and the symmetry of the crystals were examined by

Weissenberg exposures. Integrated intensities were measured by means of $\omega/2\theta$ scans on an Enraf-Nonius CAD4 diffractometer. The structures were solved by Patterson syntheses (Sn, Hal) and completed by Fourier syntheses (C, O, S). The refinements resulted in good convergences and in even distributions of the variances. Fractional atomic coordinates and equivalent isotropic thermal displacements are given in Tables 11 and 12.

Cl−(Me)Sn(SCH_2CH_2)$_2$O (**4a**) crystallizes in the noncentrosymmetric space group $P6_1$. To prove the significance of the chosen enantiomer, all coordinates were inverted and refined in $P6_5$. The ratio of the weighted R's is 1.011, which corresponds to a significance level of 99.5%. For this structure SHELX-93 was used. To refine the respective splittings of the two carbon atoms C(1) and C(2) properly, the distances S−C, C−C, and C−O were refined with the same value for each type. In addition, the isotropic temperature factors of C(1), C′(1), C(2), and C′(2) were refined together. The hydrogen atoms at the disordered atoms were calculated geometrically (U = 0.08 Å^2). Me_2Sn(SCH_2CH_2)$_2$O (**7a**) crystallizes in the centrosymmetric space group *Pnma*, in which Sn, O, and Me(eq) are located on a mirror plane. Me(ax) shows a displacement perpendicular to this mirror plane. Hydrogen atoms were calculated and refined as riding on their carbon atoms (U = 0.11 and U = 0.16 for H(Me)). All other compounds exhibit the space group $P2_1/n$. The compounds **4b,c** and **5a,c** are isostructural, respectively.

Besides several locally written routines, local versions of SHELX-76, SHELX-86, and SHELX-93 were used for the calculations and ORTEP and PLUTO for the drawings. Calculations were performed on an IBM RISC/6000.

Vibrational Spectroscopy. FT-IR spectra were recorded on a Mattson Galaxy 2030 spectrometer (samples as pressed disks with polyethylene), Raman spectra on a Spex 1403 spectrometer (excitation with a He/Ne laser at 633 nm or with a Kr laser at 647 nm; microcrystalline samples in capillaries).

Table 12. Fractional Atomic Coordinates and Equivalent Isotropic Thermal Paramters for ClMeSn(SCH_2CH_2)$_2$S (5a), BrMeSn(SCH_2CH_2)$_2$S (5b), and Me_2Sn(SCH_2CH_2)$_2$S (8a) (ESD's in Parentheses)

atom	*x/a*	*y/b*	*z/c*	*U*(eq), Å^2 [a]
		Compound **5a**		
Sn	0.02060(2)	0.15845(1)	0.20102(2)	0.03222(9)
Cl(ax)	−0.0237(1)	0.14000(7)	−0.07068(8)	0.0547(3)
Me(eq)	0.2488(3)	0.0987(2)	0.2689(4)	0.050(1)
S(1)	−0.0206(1)	0.33696(5)	0.1661(1)	0.0472(3)
C(1)	0.0312(4)	0.3870(2)	0.3556(4)	0.046(1)
C(2)	−0.0505(4)	0.3361(2)	0.4621(5)	0.050(1)
S(2)	0.02527(8)	0.20982(6)	0.50408(8)	0.0429(2)
C(3)	−0.1446(4)	0.1392(3)	0.5157(4)	0.048(1)
C(4)	−0.2627(3)	0.1243(3)	0.3673(4)	0.047(1)
S(3)	−0.18882(8)	0.05205(6)	0.23155(8)	0.0442(2)
		Compound **5b**		
Sn	0.02464(4)	0.16112(3)	0.21131(4)	0.0304(1)
Br(ax)	−0.01877(9)	0.14325(6)	−0.07118(7)	0.0536(3)
Me(eq)	0.2536(7)	0.0989(5)	0.2797(7)	0.047(2)
S(1)	−0.0160(2)	0.3390(1)	0.1764(2)	0.0463(5)
C(1)	0.0314(7)	0.03897(4)	0.3637(7)	0.043(2)
C(2)	−0.0515(8)	0.3358(5)	0.4635(8)	0.052(2)
S(2)	0.0263(2)	0.2112(1)	0.5063(2)	0.0407(5)
C(3)	−0.1418(8)	0.1396(5)	0.5206(7)	0.047(2)
C(4)	−0.2612(7)	0.1247(5)	0.3715(7)	0.045(2)
S(3)	−0.1864(2)	0.0543(1)	0.2364(2)	0.0419(5)
		Compound **8a**		
Sn	0.22220(2)	0.33302(2)	0.26890(2)	0.03555(7)
Me(ax)	0.4332(3)	0.3928(3)	0.2988(3)	0.051(1)
Me(eq)	0.1239(3)	0.2819(3)	0.0858(2)	0.049(1)
S(1)	0.10920(7)	0.53380(7)	0.32264(7)	0.0438(2)
C(1)	−0.0700(3)	0.5165(3)	0.2409(3)	0.0468(9)
C(2)	−0.1537(3)	0.4213(3)	0.2997(3)	0.048(1)
S(2)	−0.11443(8)	0.24469(7)	0.27863(7)	0.0459(2)
C(3)	−0.0568(3)	0.1860(3)	0.4335(3)	0.053(1)
C(4)	0.0874(3)	0.2297(3)	0.4973(2)	0.047(1)
S(3)	0.22103(7)	0.16694(7)	0.42761(7)	0.0450(2)

[a] $U(\text{eq}) = {}^1/_3\sum_i\sum_j U(ij)\, a_i^* a_j^* (\mathbf{a}_i \cdot \mathbf{a}_j)$.

Acknowledgment. We are grateful for financial assistance from the Deutsche Forschungsgemeinschaft, Bonn-Bad Godesberg, Germany, and from the Fonds der Chemischen Industrie, Frankfurt/Main, Germany.

Supplementary Material Available: Tables giving anisotropic thermal displacement parameters, H atom positional parameters, and all bond lengths, bond angles, and torsion angles for **4a−c**, **5a−b**, **7a** and **8a** and tables giving complete IR and Raman wavenumbers and assignments for **4a−c**, **5a−c**, **6a−c**, **7a**, **8a**, and **9a** (19 pages). Ordering information is given on any current masthead page.

OM940406I

(14) Harrison, P. G. In *Comprehensive Coordination Chemistry*; Wilkinson, G., Gillard, R. D., McCleverty, J. A., Eds.; Pergamon Press: Oxford, U.K., 1987; Vol. 3, pp 185, 197, 205.

(15) Tandura, S. N.; Voronkov, M. G.; Alekseev, N. V. *Top. Curr. Chem.* **1986**, *131*, 99. Sheldrick, W. S. In *The Chemistry of Organic Silicon Compounds*; Patai, S., Rappoport, Z., Eds.; Wiley: Chichester, U.K., 1989; Part 1, p 279. Corriu, R. J. P.; Young, J. C. In *The Chemistry of Organic Silicon Compounds*; Patai, S., Rappoport, Z., Eds.; Wiley: Chichester, U.K., 1989; Part 2, p 1241. Corriu, R.; Guérin, C.; Henner, B.; Wang, Q. *Inorg. Chim. Acta* **1992**, *198−200*, 705.

(16) Rivière, P.; Rivière-Baudet, M.; Satgé, J. In *Comprehensive Organometallic Chemistry*; Wilkinson, G., Stone, F. G. A., Abel, E. W., Eds.; Pergamon Press: Oxford, U.K., 1982; Vol. 2, p 502.

(17) Dräger, M. *Z. Anorg. Allg. Chem.* **1976**, *423*, 53.

(18) Harrison, P. G. In *Comprehensive Organometallic Chemistry*; Wilkinson, G., Stone, F. G. A., Abel, E. W., Eds.; Pergamon Press: Oxford, U.K., 1982; Vol. 2, p 630.

(19) Pyykkö, P. *Chem. Rev.* **1988**, *88*, 563.

(20) Bassindale, A. R.; Taylor, P. G. In *The Chemistry of Organic Silicon Compounds*; Patai, S., Rappoport, Z., Eds.; Wiley: Chichester, U.K., 1989; Part 1, p 839. Holmes, R. R. *Chem. Rev.* **1990**, *90*, 17.

(21) Corriu, R. J. P. *J. Organomet. Chem.* **1990**, *400*, 81. Chuit, C.; Corriu, R. J. P.; Reye, C.; Young, J. C. *Chem. Rev.* **1993**, *93*, 1371.

(22) Dräger, M.; Guttmann, H.-J. *J. Organomet. Chem.* **1981**, *212*, 171.